Visible Infrared Imaging Radiometer Suite (VIIRS) 375 m Active Fire Detection and Characterization Algorithm Theoretical Basis Document 1.0

December 2016

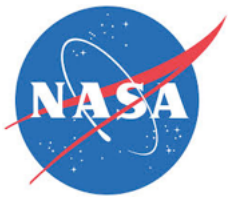

Table of Contents

Written by:

Wilfrid Schroeder & Louis Giglio
Department of Geographical Sciences
University of Maryland
Email: wschroed@umd.edu

1. SCIENCE RATIONALE FOR THE PRODUCT

This document describes the Visible Infrared Imaging Radiometer Suite (VIIRS) 375 m active fire detection product. The VIIRS instrument was first launched on 28 October 2011 onboard the Suomi National Polar-orbiting Partnership (S-NPP), which was placed in a sun synchronous orbit at an altitude of 829 km and with 1:30pm/1:30am equatorial crossing times. That instrument will be followed by other similar sensors onboard the Joint Polar Satellite System (JPSS) series of satellites operated jointly by NASA and NOAA. VIIRS is a whiskbroom scanning radiometer with a swath width of 3060 km, providing global wall-to-wall coverage every 12 h or less depending on the latitude. It consists of a multispectral instrument including five spectral channels (0.6 <> 12.4 μm) at 375 m (I-bands) and 16 spectral channels (0.4 <> 12.5 μm) at 750 m (M-bands), in addition to a light-sensitive (0.5 <> 0.9 μm) day-and-night band at 750 m (DNB).

Compared to other coarser resolution (≥1 km) satellite fire detection products, the VIIRS 375 m data provide greater response over fires of relatively small area, as well as improved mapping of large fire perimeters. Consequently, the data are well suited for use in support of fire management (e.g., near real-time wildfire alert systems), as well as other science applications requiring improved fire mapping fidelity. This product consists of a hybrid algorithm combining qualities of the 375 m and 750 m VIIRS data. The higher resolution data (channels I1-I5) are the primary drivers of the fire detection component, whereas the 750 m data (specifically the dual-gain M13 channel) are used primarily in the sub-pixel fire radiative power (FRP) retrievals. The 375 m fire algorithm supersedes the baseline VIIRS 750 m active fire detection and characterization data, which was originally designed to provide continuity to the 1 km Earth Observing System Moderate Resolution Imaging Spectroradiometer (EOS/MODIS) active fire data record.

2. THE ALGORITHM

2.1. TECHNICAL BACKGROUND AND HERITAGE

Actively burning fires often show a wide range of temperatures spanning several hundred Kelvin in association with flaming and smoldering phases of combustion. Typically, cooler smoldering fires show temperatures between 450 and 850 K, whereas higher temperatures ranging from 800 K to upwards of 1200 K prevail during the more intense flaming phase [Lobert and Warnatz, 1993]. Fuel type and moisture, and ambient conditions (air temperature, wind, and relative humidity) are key factors regulating biomass combustion. When moderate spatial resolution sensors are considered, mid-infrared (4 μm) spectral channels are the most responsive to actively burning fires capturing most of the radiometric signal from smoldering and flaming phases of combustion during both day and nighttime parts of the orbit. The peak in emitted fire radiant energy on channel I4 makes that channel (and similarly channel M13) responsive to small sub-pixel fires occurring over a cool (≤ 300 K) background. Consequently, intense active fires (>1000 K)

occupying fractional pixel areas as small as 10^{-4} may be detected. In addition to facilitating the detection of sub-pixel active fires, the rate of radiative energy released by fires observed in the 4 μm region is found to be directly related to the biomass consumed per unit time [Kaufman *et al*., 1998; Wooster *et al*., 2003].

The VIIRS active fire detection data build on the EOS/MODIS fire product heritage using a multi-spectral contextual algorithm to identify sub-pixel fire activity and other thermal anomalies in the Level 1 (swath) input data [Kaufman *et al*., 1998]. The baseline VIIRS 750 m active fire detection product was originally designed mirroring the MODIS Collection 4 *Fire and Thermal Anomalies* algorithm (MOD14/MYD14), although lacking key output science data layers such as the 2D fire mask and FRP retrievals [Csiszar *et al*., 2014; Giglio *et al*., 2003]. That algorithm was later replaced with the MODIS Collection 6 algorithm equivalent including all output science data layers [Giglio *et al*., 2016]. That product is available through various VIIRS data outlets providing direct readout (NASA's International Polar Orbiter Processing Package [IPOPP]), near real-time (NOAA's S-NPP Data Exploitation [NDE]), and science data access (NASA's Land Science Investigator-led Processing System [Land SIPS]). The VIIRS 750 m fire product generation and availability will continue until further notice.

The algorithm described in this document was proposed during the early post-launch period following the successful application of the 375 m data for active fire detection. That new application constituted a repurposing of the VIIRS 375 m (I) channels, as none of those were originally designed for active fire detection. Most importantly, abnormal radiometric conditions involving different pixel saturation scenarios are frequently observed in the primary mid-infrared channel I4 thereby requiring special handling of the data. Building on the MOD14/MYD14 algorithm, several modifications were implemented in order to accommodate the unique characteristics associated with the VIIRS 375 m data. Detailed algorithm description is provided in the following sections. The information contained in this document is complemented by the original peer-reviewed publication describing the initial implementation of the VIIRS 375 m global algorithm [Schroeder *et al*., 2014].

2.2. ALGORITHM INPUT

The VIIRS 375 m fire product uses input data from all five 375 m channels (I1-I5) and the dual-gain 750 m mid-infrared data (channel M13), in addition to their corresponding quality flags (QF1) (Table 1). The product evolved from the Schroeder *et al*. [2014] VIIRS 375 m global fire algorithm, incorporating an ancillary land-water classification mask, FRP retrievals based on the methodology described in Wooster *et al*. [2003], among other refinements. The higher resolution VIIRS 375 m data provide the basis for the detection of active fires and other thermal anomalies, whereas the 750 m data are used in the calculation of sub-pixel FRP as well as to discriminate potential false alarms associated with noise in the input fire-sensitive 375 m mid-infrared (I4) channel data.

Table 1: List of VIIRS channels used as input to the 375 m active fire detection algorithm. The corresponding VIIRS Level 1B data quality flags, terrain-corrected geolocation and quarterly land-water mask data complement the list of input files used.

Channel	Spatial Resolution (m)	Spectral resolution (µm)	Primary Use
I1	375	0.60 – 0.68	Cloud & water classification
I2	375	0.846 – 0.885	Cloud & water classification
I3	375	1.58 – 1.64	Water classification
I4	375	3.55 – 3.93	Fire detection
I5	375	10.5 – 12.4	Fire detection & cloud classification
M13*	750	3.973 – 4.128	FRP retrieval, fire detection over water and across the South Atlantic magnetic anomaly region

* Aggregated (750×750 m nominal) & un-aggregated (250×750 m nominal) data are used

The 375 m data describe the nominal resolution after native pixels are spatially aggregated (Figure 1). The aggregation scheme changes across three distinct image regions. In the first region (nadir to 31.59^o scan angle), three native pixels are aggregated in the along scan (cross-track) direction to form one data sample in the Level 1 image. In the second region (31.59^o to 44.68^o scan angle), two native pixels are aggregated to form one data sample. Finally in the third and last region (44.68^o to 56.06^o - edge of swath) one native pixel will result in one data sample. All five 375 m channels are aggregated onboard the spacecraft before the data are transmitted to the ground stations. The input 750 m dual-gain M13 channel data undergo a similar aggregation scheme although the data reduction is performed after the ground stations receive the native resolution data from the satellite. In order to maximize performance, the algorithm uses both aggregated and un-aggregated M13 data.

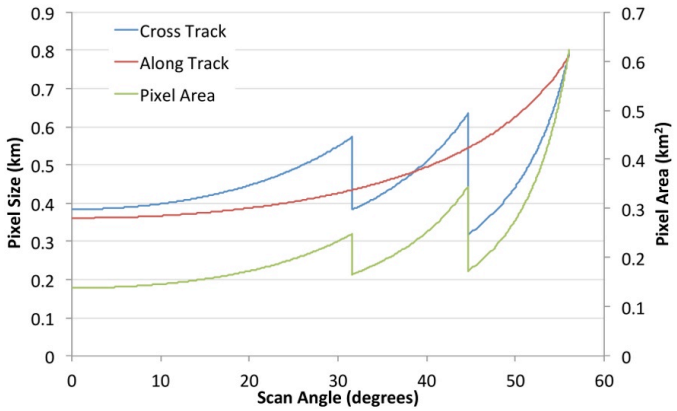

Figure 1: Spatial resolution of VIIRS imager data (I bands) as a function of scan angle. The three distinct regions describe data aggregation zones extending from nadir to the edge of the swath.

Given the unique spatial and spectral resolution of the data, the fire detection algorithm was customized and tuned in order to optimize its response over small fires while balancing the occurrence of false alarms. Frequent saturation of the mid-infrared I4 channel driving the detection of active fires demands additional tests and procedures in order to avoid pixel classification errors. Pixel saturation occurs most

often over large and/or intense heat sources (e.g., wildfires) and is typically identified in the input data with the use of the companion quality flag. Under more extreme conditions, very large active fires (e.g., crown fires) can greatly exceed the effective saturation temperature on channel I4 leading to a complete folding of the digital number (DN) associated with the affected pixel. Application of the normal calibration parameters to those anomalous DN values results in abnormally cold brightness temperature values equal to or near the low end of that channel's dynamic range (208 K). The companion quality flags may also be used to properly identify and process those pixels. A third and more challenging scenario describing channel I4 saturation involves the mixing of saturated and unsaturated data during onboard aggregation. Such occurrences result in artificially low brightness temperatures accompanied by nominal quality flags for the affected pixels. Under those conditions, complementary channel I5 data may be used to try and identify the corrupted channel I4 pixels. Overall, the low (≈358 K) effective saturation temperature on channel I4 results in ≈9% discernable fire pixel saturation rate associated with all three scenarios above (in addition to a yet unknown percentage of more subtle and therefore indistinguishable saturation). Consequently, sub-pixel fire characterization should be avoided in that channel. That limitation is addressed in the product with the use of co-located M13 dual-gain channel data. The combination of higher (≈659 K) saturation temperature and lower spatial resolution results in extremely rare pixel saturation occurrence in the M13 data making it suitable for such application.

Another anomalous condition affecting the I4 channel involves the occurrence of spurious brightness temperature data as a result of the South Atlantic magnetic anomaly. The geographic area where the problem is most commonly found extends from 110°W <> 11°E and 7°N <> 55°S (Cabrera *et al*., 2005; Casadio *et al*., 2012). The impact of the magnetic anomaly is evidenced by artificially high brightness temperature values occurring predominantly in the nighttime I4 channel data. These occurrences are typically associated with nominal data quality and therefore cannot be readily identified using the available quality flags. On average, individual channel I4 pixels affected by the anomaly may depart from the background by 15–30 K thereby creating similar radiometric responses associated with actual nighttime fire-affected pixels at both absolute and contextual levels. No discernable impact on nighttime I5 channel data quality was found associated with the magnetic anomaly.

Currently, processing of the fire algorithm is limited to the Level 2 (swath) product output, which has similar data structure and format to MODIS Level 2 (MOD14/MYD14) fire product. It includes a two-dimensional fire mask and quality assurance science data sets, plus sparse arrays describing individual fire pixel information (e.g., FRP) and additional granule attributes. Alternative text (ASCII) files are generated for each Level 2 granule containing basic fire detection information in a Geographic Information System (GIS)-friendly format. Supplementary Level 3 (tiled) and 4 (Climate Modeling Grid) product outputs will be added in the future.

2.3. ALGORITHM DESCRIPTION

The VIIRS fire algorithm uses a combination of fixed and contextual tests to detect active fires and other thermal anomalies in both daytime and nighttime (solar zenith angle ≥90°) parts of the orbit. The current implementation evolved from the work of Schroeder *et al*. (2014), incorporating new elements in response to users' requirements (e.g., sub-pixel FRP retrievals). The detection criteria are based on multi-spectral tests using primarily the mid-infrared (channel I4) and long wave-infrared (channel I5) data, complemented by cloud and water classification schemes as described below.

2.3.1. CLOUD AND WATER PIXEL CLASSIFICATION

The cloud classification scheme builds on the MODIS fire product [Giglio *et al*., 2003; 2016] and is designed to mask optically thick clouds. The resulting cloud mask is made intentionally liberal in order to minimize fire detection omission errors under translucent clouds (e.g., cirrus) and in partially covered pixels. Cloud-covered pixels are identified in the daytime data using the following criteria:

$BT_5 < 265$ K
OR
$\rho_1+\rho_2 > 0.9$ AND $BT_5 < 295$ K
OR
$\rho_1+\rho_2 > 0.7$ AND $BT_5 < 285$ K

where ρ_i and BT_i are the top-of-atmosphere reflectance and brightness temperature in VIIRS 375 m channel *i*, respectively. Nighttime cloud pixels are identified using:

$BT_5 < 265$ K AND $BT_4 < 295$ K

Pixels identified as clouds skip any subsequent fire detection processing and are also excluded from background characterization. Complementing the cloud masking, water pixels are classified using:

$\rho_1 > \rho_2 > \rho_3$

The test above can successfully mask most water bodies in the daytime data although it tends to omit sediment-filled water pixels along shorelines, and cause commission errors over burn scars. Those limitations have no observable impact on the overall fire pixel detection and characterization performance. The internal water mask complements the available VIIRS land-water mask which builds on the MODIS 250 m water classification product [Carroll *et al*., 2009]. All water pixels undergo subsequent processing to allow detection of gas flares and other thermal anomalies.

2.3.2. FIXED THRESHOLD TESTS

Fire pixels are first identified in the day and nighttime data using a combination of fixed threshold tests based on the observation scenario. Fire pixels detected using these tests show a stronger radiometric signature in either channel I4 or I5 data, and tend to be unequivocally associated with active fires or high intensity thermal anomalies. Fire pixels detected using these tests are initially assigned a '*high confidence*' class. In case of unsaturated nighttime data, the following test is used:

$BT_4 > 320$ K AND $QF_4 = 0$ (*nighttime only*)

Where QF_4 is the VIIRS channel I4 quality flag value. Saturated daytime and nighttime fire pixels are identified using the following criteria:

$BT_4 = 367$ K AND $QF_4 = 9$ AND $QF_5 = 0$ (*daytime or nighttime*)
AND
$BT_5 > 290$ K AND $\rho_1 + \rho_2 < 0.7$ (*daytime only*)

Finally, cases involving folding of channel I4 data are identified using:

$\Delta BT_{45} < 0$ AND $BT_5 > 325$ K AND $QF_5 = 0$ (*daytime only*)
OR
$\Delta BT_{45} < 0$ AND $BT_5 > 310$ K AND $QF_5 = 0$ (*nighttime only*)
OR
$BT_4 = 208$ K AND $BT_5 > 335$ K (*nighttime only*)

Where ΔBT_{45} is the brightness temperature difference between channels I4 and I5.

2.3.3. POTENTIAL BACKGROUND FIRES

Potential background fire pixels can affect the detection and characterization of individual fire pixels and therefore must be identified and masked out accordingly. The following tests are used to identify those pixels:

$BT_4 > 335$ *K* AND $\Delta BT_{45} > 30$ K (*daytime only*)
OR
$BT_4 > 300$ *K* AND $\Delta BT_{45} > 10$ K (*nighttime only*)

In addition to the tests above, pixels associated with folding of channel I4 data (typically characterized by artificially low BT_4) are also considered background pixels.

2.3.4. AVOIDING BRIGHT REFLECTIVE TARGETS

Solar reflection over bright surfaces (e.g., sand banks along riverbeds) can induce high brightness temperatures on channel I4 daytime data, causing potential

confusion with active fires. Those areas are identified and avoided using the following criteria:

$\rho_3 > 0.3$ AND $\rho_3 > \rho_2$ AND $\rho_2 > 0.25$ $BT_4 \leq 335$ K

Sun glint is a form of recurring observation phenomenon also known to lead to false alarms in satellite fire detection products. Examples of false alarm-prone areas associated with solar reflection include large metallic rooftops in industrial parks, small/undetected water bodies, and other bright surfaces in urban areas. In order to reduce the frequency of those occurrences, pixels identified with the following tests are assigned a '*sun glint*' class and not considered for candidate fire pixel selection (Section 2.3.5):

$cos\theta_g = cos\theta_v \times cos\theta_s - sin\theta_v \times sin\theta_s \times cos\phi$

$\theta_g < 15^o$ AND $\rho_1 + \rho_2 > 0.35$
OR
$\theta_g < 25^o$ AND $\rho_1 + \rho_2 > 0.4$

Where θ_v and θ_s are the view and solar zenith angles, respectively, and ϕ is the relative azimuth angle.

2.3.5. CANDIDATE FIRE PIXELS

Candidate fire pixels are selected using relatively liberal tests in order to include all potential pixels showing thermal anomalies on channel I4 according to:

$BT_4 > BT_{4S}$ AND $\Delta BT_{45} > 25$ K (*daytime only*)
OR
$BT_4 > 295$ K AND $\Delta BT_{45} > 10$ K (*nighttime only*)

Where BT_{4S} is a dynamically-adjusted background value calculated using channel I4 brightness temperature data based on a 501×501 sampling window centered on the candidate fire pixel. This initial large-area sampling accommodates variations in background conditions, adding flexibility to candidate fire pixel selection. It is intended to improve algorithm sensitivity to fires occurring in colder high latitude regions, while reducing false alarm rates in lower latitudes consisting of warmer background. The large area background sampling excludes all pixels previously classified as cloud, water bodies, and potential background fire pixels, as well as any pixel with non-zero quality flag including fill values associated with *bowtie* deletion samples [Wolfe *et al*., 2013]. BT_{4S} is defined as:

$BT_{4M} = MAX[325, M+25]$ K
$BT_{4S} = MIN[330, BT_{4M}]$ K

Where M is the BT_4 median value calculated for the 501×501 window. The sampling window must contain a minimum of 10 valid observations otherwise BT_{4S} is set to 330 K. Furthermore, BT_{4S} is only derived for daytime data allowing the candidate fire pixel brightness temperature on channel I4 to vary between a minimum of 325 K to a maximum of 330 K in order to accommodate scene-dependent changes in background conditions. Nighttime background conditions are found to be less variable, therefore the algorithm uses a single fixed value to define candidate fire pixels at night.

2.3.6. CONTEXTUAL FIRE DETECTION TESTS

The contextual tests use a dynamic sampling window to characterize the background conditions around each individual candidate fire pixel. The sampling window is allowed to vary from a minimum of 11×11 elements centered on the candidate pixel, to a maximum of 31×31 elements until ≥25% or ≥10 valid pixels are encountered. Valid pixels exclude clouds, background fire pixels, non-nominal quality data, and are limited to same-class pixels (i.e., candidate fire pixels over land (water) use land (water) background pixels only). Candidate fire pixels lacking proper background characterization are assigned the "*unclassified*" class. Daytime candidate fire pixels having ≥4 background fire pixels in the sampling window, or having background fire pixels in excess of 10% of the valid background pixels must go through the following test:

$\rho_2 > 0.15$ AND $BT'_{4B} < 345$ K AND $\delta'_{4B} < 3$ K *AND* $BT_4 < BT'_{4B} + 6 \times \delta'_{4B}$

Where BT'_{4B} and δ'_{4B} are the mean brightness temperature and mean absolute deviation, respectively, calculated using the potential background fire pixels. Candidate fire pixels that satisfy the criteria above are excluded from further processing and assigned a fire-free (water or land) pixel class. The tests below describe the subsequent daytime and nighttime data processing criteria applied to the remaining candidate fire pixels:

Daytime:
$\Delta BT_{45} > \Delta BT_{45B} + 2 \times \delta_{45B}$
AND
$\Delta BT_{45} > \Delta BT_{45B} + 10$ K
AND
$BT_4 > BT_{4B} + 3.5 \times \delta_{4B}$
AND
$BT_5 > BT_{5B} + \delta_{5B} - 4$ K OR $\delta'_{4B} > 5$ K

Nighttime:
$\Delta BT_{45} > \Delta BT_{45B} + 3 \times \delta_{45B}$
AND
$\Delta BT_{45} > \Delta BT_{45B} + 9$ K

AND
$BT_4 > BT_{4B} + 3 \times \delta_{4B}$

Where ΔBT_{45B} and BT_{iB} denote the mean channel I4-I5 brightness temperature difference and the mean brightness temperature on channel *i*, respectively, calculated using the valid background pixels; δ_{45B} and δ_{4B} are the mean absolute deviation calculated for channel I4-I5 brightness temperature difference and channel I4, respectively, also using the valid background pixel data. Candidate fire pixels meeting the criteria above are assigned a '*nominal'* confidence fire pixel class.

2.3.7. SECONDARY TESTS

Two additional tests are applied to the data in order to (i) identify residual fire pixels not detected with the criteria above, and (ii) mark down potential low confidence fire pixels.

The first test targets less common pixel saturation and folding scenarios using the following criteria:

$BT_5 \geq 325$ K OR $BT_4 = 355$ K OR $\Delta BT_{45} < 0$ K

Pixels that meet such criteria and have one or more adjacent fire pixels of '*nominal*' or '*high*' confidence (among the eight immediate neighbors) are assigned a '*low'* confidence fire class.

The second test targets residual false alarms occurring along Sun glint areas. The following test is applied to all '*nominal confidence*' fire pixels:

$\Delta BT_{45} \leq 30$ K OR $\theta_g < 15^o$

Pixels meeting the above criteria will be assigned a '*low confidence*' fire pixel class if one of the following conditions apply:

(i) two or more adjacent '*Sun glint*' pixels are found
(ii) no adjacent '*high confidence*' pixels are found and BT_4 is less than 15 K higher than adjacent pixels

2.3.8. NIGHTTIME SOUTH ATLANTIC MAGNETIC ANOMALY FILTER

Noise associated with the South Atlantic magnetic anomaly is particularly pronounced in the mid-infrared channel I4 data driving the detection of fires and thermal anomalies. The noise condition is found predominantly at night, with only few and sparse occurrences during the day. Given the random nature and radiometric signal characteristics of the resulting channel I4 noise, which often mimic those of actual fires, several spurious fire pixels are normally produced over the affected region (Figure 2). Data artifacts are often linked to single, stand-alone pixels showing abnormally high brightness temperature on channel I4. In order to address the problem, the algorithm uses co-located un-aggregated M13 brightness

temperature data to independently verify nighttime fire pixels. Despite their similar spectral characteristics, channel M13 shows significantly lower rates of data contamination compared to channel I4. In addition to that, channel I4 and M13 occurrences are found to be predominantly independent from each other.

The filter first creates a modified aggregated M13 data array by replacing the mean value aggregation scheme with a maximum value method. This approach minimizes fire signal loss as a result of the normal aggregation scheme. The suspicious 375 m fire pixel is subsequently co-located to the modified M13 data array, after which the coincident M13 aggregated pixel is selected for further analysis. In order to be confirmed as a '*nominal*' or '*high*' confidence fire pixel, the coincident M13 pixel brightness temperature must be ≥ 2 K than all of the adjacent M13 pixels. Pixels that failed that test are downgraded to a fire-free ('*water*' or '*land*') class and marked with a unique quality flag (see Table 3).

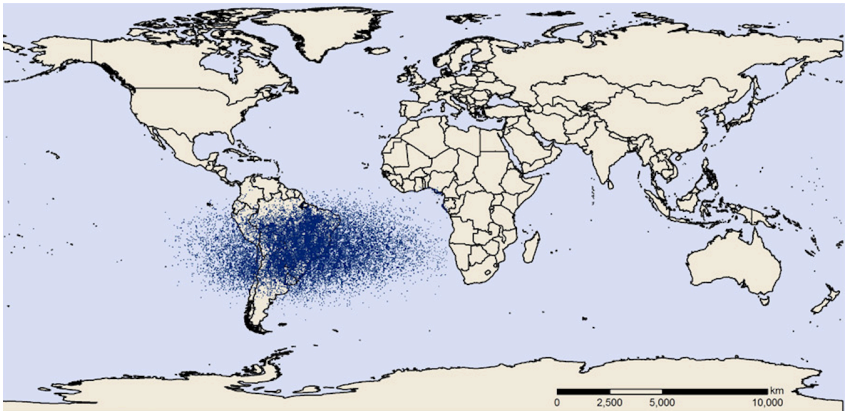

Figure 2: Spurious VIIRS 375 m fire detections associated with the South Atlantic magnetic anomaly during 01-30 August 2013 (adapted from Schroeder *et al*. [2014]).

2.3.9. PERSISTENCE TEST

Some residual noise in the input data may propagate through the algorithm leading to few and isolated spurious detections most easily found over ocean waters. Such cases are typically associated with random sensor noise or with infrequent manifestation of South Atlantic magnetic anomaly on daytime data. In order to improve handling of those cases, the algorithm includes a persistence test applied to fire pixels detected over water. Based on that test, '*low*', '*nominal*' and '*high*' confidence fire pixels detected over water must show distinguishable heat signature on channel M13. The test uses the same approach and modified M13 aggregated data array described in Section 2.3.8, requiring a slightly higher brightness temperature difference of 2.5 K between the target M13 pixel and the adjacent ones. Pixels failing that initial test must show temporal persistence consisting of a minimum of 3 co-located detections in the previous 30 days in order to be confirmed. Pixels lacking M13 channel heat signature or persistence indication are downgraded to fire-free ('*water*' or '*land*') pixels and marked up with unique quality flags (bits 19-21 on Table 3).

2.3.10. FIRE RADIATIVE POWER RETRIEVAL

Because of the frequent fire pixel saturation in the mid-infrared I4 channel, fire radiative power retrievals are calculated using co-located M13 channel data. The approach utilizes 375 m data to identify fire pixels and to assist in the selection of valid background pixels. Co-located M13 aggregated radiances coinciding with the fire-affected and background pixels are used in the FRP retrieval following Wooster *et al*. [2003], which is represented by (assuming unit atmospheric transmittance and surface emissivity):

$$FRP = \frac{A\sigma(L_{13} - L_{13B})}{a}$$

Where A is the pixel area which varies as a function of scan angle, σ is the Stefan-Boltzmann constant (5.67×10^{-8} $Wm^{-2}K^{-4}$), a is a channel-specific constant (VIIRS M13 = 2.88×10^{-9} $Wm^{-2}sr^{-1}\mu m^{-1}K^{-4}$), and L_{13} and L_{13B} are the M13 channel fire pixel and mean background radiances, respectively. Despite being extremely rare, M13 pixel saturation may occur over very large and intense active fires. Normally, that condition will trigger the appropriate quality flag for the affected pixel in the input data, which may carry a fill (non-usable) radiance value. In that event, the fire pixel may still be detected (granted that the algorithm is able to resolve it using the available data) whereas the FRP retrieval will be set to zero. Other situations involving challenging FRP retrieval (e.g., insufficient background data) may also result in fire pixels accompanied by null FRP values. We note that such cases are rather infrequent. A single pixel 750 m FRP retrieval is divided among the number of coincident 375 m fire pixels, with each sub-pixel receiving the same resulting value in MW (Figure 3).

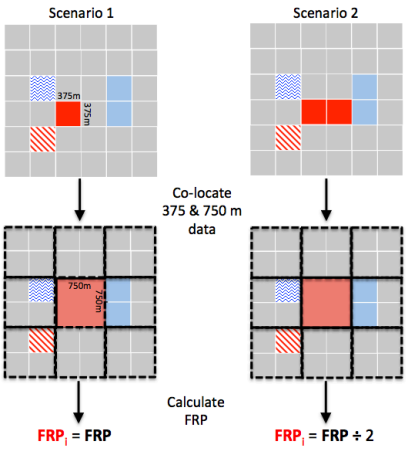

Figure 3 FRP calculation using a combination of VIIRS 375 m and 750 m data. The former is used to identify fire-affected (solid and dashed red), cloud (solid blue), water pixels (dashed blue), and valid background pixels (gray; in this case representing fire-free land surface). Co-located M13 channel radiance data (750 m; black dashed outline) coinciding with fire pixel (red shade) and valid background pixels (gray-only) are used in the FRP calculation. In scenario 1, the single 750 m retrieval (center pixel; **FRP**) is assigned to the single coincident 375 m fire pixel (solid red; **FRP$_i$**, where *i* is the 375 m fire-affected sub-pixel index). In scenario 2, the single 750 m FRP retrieval is split between the two coincident 375 m fire-affected sub-pixels, so that **FRP$_i$** = **FRP**÷2.

3. PRODUCT DESCRIPTION

The VIIRS land product suite is composed of Level 2 (swath projection), Level 3 (tiled, with some multi-temporal data), and Level 4 (gridded data meeting climate modeling community requirements) data sets. Currently, the active fire data set is restricted to Level 2 processing carrying similar characteristics as the input L1B data ingested by the algorithm. The data are stored in swath projection with individual granules comprising an orbit segment of approximately 6 min. VIIRS Level 3 & 4 fire data products should become available in the near future.

3.1. LEVEL 2 ACTIVE FIRE DATA

3.1.1. FILE FORMAT

VIIRS active fire data are output in NetCDF4.2 file format. Level 2 files also share several of the L1B global attributes (including nomenclature); files can be manipulated using standard NetCDF-enabled software. Filename convention is as follows:

VNP14IMG.AYYYYDDD.HHMM.VVV.yyyydddhhmmss.nc
Where:
VNP14IMG = VIIRS 375 m active fire product identifier
YYYY = year of data acquisition
DDD = Julian day of data acquisition
HHMM = hour and minute of data acquisition
yyyydddhhmmss = data processing time (year, Julian day, hour, minute, second)

3.1.2. DATA CONTENT

The VIIRS active fire algorithm output contains 25 primary science data sets, in addition to the algorithm's quality flag (see Section 3.2). The individual science data sets (SDSs) are named as follows:

'*fire mask*' = image classification array (2D)
'*FP_line*' = granule line of fire pixel
'*FP_sample*' = granule sample of fire pixel
'*FP_latitude*' = latitude of fire pixel (degrees)
'*FP_longitude*' = longitude of fire pixel (degrees)
'*FP_T4*' = channel I4 brightness temperature of fire pixel (kelvin)
'*FP_T5*' = channel I5 brightness temperature of fire pixel (kelvin)
'*FP_MeanT4*' = channel I4 mean background brightness temperature (kelvin)
'*FP_MeanT5*' = channel I5 mean background brightness temperature (kelvin)
'*FP_MeanDT*' = mean background I4-I5 brightness temperature difference (kelvin)
'*FP_MAD_T4*' = background channel I4 brightness temperature mean absolute deviation (kelvin)
'*FP_MAD_T5*' = background channel I5 brightness temperature mean absolute deviation (kelvin)

'*FP_MAD_DT*' = background I4-I5 brightness temperature difference mean absolute deviation (kelvin)
'*FP_power*' = fire radiative power (MW)
'*FP_M13*' = channel M13 radiance of fire pixel ($W.m^{-2}.sr^{-1}.\mu m^{-1}$)
'*FP_MeanM13*'= channel M13 mean background radiance ($W.m^{-2}.sr^{-1}.\mu m^{-1}$)
'*FP_AdjCloud*' = number of adjacent cloud pixels
'*FP_AdjWater*'= number of adjacent water pixels
'*FP_WinSize*' = number of adjacent water pixels
'*FP_confidence*'= detection confidence (7=low, 8=nominal, 9=high)
'*FP_day*' = day flag for fire pixel (0=night, 1=day)
'*FP_SolZenAng*'= solar zenith angle of fire pixel (degrees)
'*FP_SolAzAng*'= solar azimuth angle of fire pixel (degrees)
'*FP_ViewZenAng*'= view zenith angle of fire pixel (degrees)
'*FP_ViewAzAng*' = view azimuth angle of fire pixel (degrees)

The '*fire mask*' SDS consists of an 8-bit integer two-dimensional array with the same number of elements as the input L1B data array (Figure 4). Fire masks generated from the standard 6-minute files have 6,400 samples (constant) and 202 <> 203 scans totaling 6,464 <> 6,496 rows (variable number of scans per granule is designed to accommodate ≈6 minute data segments). Distinct pixel classes are used for land, water, cloud and fire pixels, plus additional classes indicating non-processed pixels and pixels with undefined classification ('*unclassified*') (Table 2). The latter describes those cases when background statistics cannot be retrieved preventing proper pixel classification. Fire pixel confidence classes ('*low*', '*nominal*' and '*high*') are representative of the observation conditions associated with each detection (see Section 2). The additional data sets output by the algorithm consist of individual sparse arrays containing image line, column, longitude, latitude, FRP, detection confidence, among other parameters for all fire pixels detected.

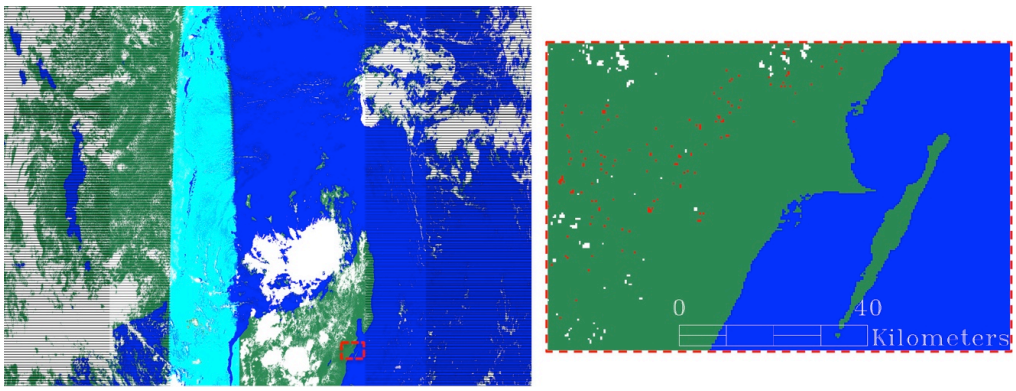

Figure 4: S-NPP/VIIRS 375 m active fire detection classification product (mask) derived for a granule acquired on 22 November 2015 at 1035UTC over parts of northern Madagascar and southeast Africa (left). Right panel shows magnified subset containing land (green), water (blue), clouds (white) and fire (red) pixels. Glint (cyan) and *bowtie* deletion (black) pixels are also visible in the large image.

Table 2: VIIRS 375 m '***fire mask***' data set classes.

Pixel Class	Definition
0	Not processed
1	*Bowtie* deletion
2	Sun glint
3	Water
4	Clouds
5	Land
6	Unclassified
7	Low confidence fire pixel
8	Nominal confidence fire pixel
9	High confidence fire pixel

3.2. QA/METADATA

A two-dimensional array complements the fire mask output providing quality assurance (QA) information for every pixel processed. The QA data are stored in 32-bit unsigned integer format populated with several fields that together can be used to reconstruct some of the key observation conditions pertinent to each pixel analyzed. Bits 0-6 describe the overall (nominal/non-nominal) quality of all input files used, followed by bits 7-18 describing primary and secondary fire detection tests. Bits 19-22 are used to mark pixels associated with detection over water (persistence test) and/or *bowtie* conditions, whereas bit 23-31 are reserved for future use.

Table 3: VIIRS 375 m fire detection '*algorithm QA*' data set bits and definition.

Bit	Description
0	Channel I1 quality (0 = nominal (or nighttime), 1 = non-nominal)
1	Channel I2 quality (0 = nominal (or nighttime), 1 = non-nominal)
2	Channel I3 quality (0 = nominal (or nighttime), 1 = non-nominal)
3	Channel I4 quality (0 = nominal, 1 = non-nominal)
4	Channel I5 quality (0 = nominal, 1 = non-nominal)
5	Geolocation data quality (0 = nominal, 1 = non-nominal)
6	Channel M13 quality (0 = nominal, 1 = non-nominal)
7	Unambiguous fire (0 = false, 1 = true [night only])
8	Background pixel (0 = false, 1 = true) BT_4 > 335 K AND ΔBT_{45} > 30 K OR saturation/folding (day) BT_4 > 300 K AND ΔBT_{45} > 10 K OR saturation/folding (night)
9	Bright pixel rejection (0 = false, 1 = true) ρ_3 > 30% AND ρ_3 > ρ_2 AND ρ_2 > 25% AND $BT_4 \leq$ 335K
10	Candidate pixel (0 = false, 1 = true) BT_4 > 325 K AND ΔBT_{45} > 25 K (daytime) BT_4 > 295 K AND ΔBT_{45} > 10 K (nighttime)
11	Scene background (0 = false, 1 = true) BT_4 > MIN([330, BT_{4M}]) (day)
12	Test 1 (0 = false, 1 = true) ΔBT_{45} > ΔBT_{45B} +2×δ_{45B} (day) ΔBT_{45} > ΔBT_{45B} +3×δ_{45B} (night)
13	Test 2 (0 = false, 1 = true) ΔBT_{45} > ΔBT_{45B} +10 K (day) ΔBT_{45} > ΔBT_{45B} +9 K (night)

14	Test 3 (0 = false, 1 = true) $BT_4 > BT_{4B} + 3.5 \times \delta_{4B}$ (day) $BT_4 > BT_{4B} + 3 \times \delta_{4B}$ (night)
15	Test 4 (0 = false, 1 = true) (day) $BT_5 > BT_{5B} + \delta_{5B} - 4$ K OR $\delta'_{4B} > 5$ K
16	Pixel saturation condition (0 = false, 1 = true) (day) $BT_5 \geq 325$ K OR $BT_4 = 367$ K OR $\Delta BT_{45} < 0$
17	Glint condition (0 = false, 1 = true) (day) $\Delta BT_{45} \leq 30$ K OR Glint (θ_g) < 15°
18	Potential South Atlantic magnetic anomaly pixel (0 = false, 1 = true)
19	Fire pixel over water (0 = false, 1 = true)
20	Persistence test (0 = false, 1 = true) BT_{13}-MAX[BT_{13B}] < 2.5 K
21	Persistence test (0 = false, 1 = true) Number of previous co-located detections < 3
22	Residual *bowtie* pixel (0 = false, 1 = true)
23-31	Reserved for future use

4. PRODUCT ASSESSMENT

4.1. THEORETICAL FIRE DETECTION CURVES

A theoretical fire detection envelope was calculated by simulating different fire scenarios applied to actual VIIRS 375 m global imagery. Fires were simulated assuming areas ranging from 2 to 250 m^2, and temperatures ranging from 400 to 1200 K. Fire radiances were derived at 2 m^2 and 10 K intervals for both I4 and I5 channels using the instrument's spectral response functions, and assuming blackbody emission. A total of 10 daytime and 10 nighttime VIIRS L1B granules acquired during August 2013 were randomly selected covering different geographic areas, including low and high latitude regions, with variable levels of fire activity. For every image, 10 pixels were selected along nadir and apart from each other, and when possible, near areas of fire activity in order to best represent regional fire-prone conditions. Simulated fire radiances and actual background radiances were area-weighted to provide realistic BT_4 and BT_5 pixel values representative of actual observation conditions. The active fire detection algorithm was then applied to the data containing simulated active fire pixel surrounded by genuinely observed background pixels. Figure 5 shows the 50% probability of detection curves derived for the algorithm using the global daytime and nighttime data sample. Improved nighttime performance resulted from the more homogeneous background conditions, which tends to enhance the algorithm's response to relatively small heat sources.

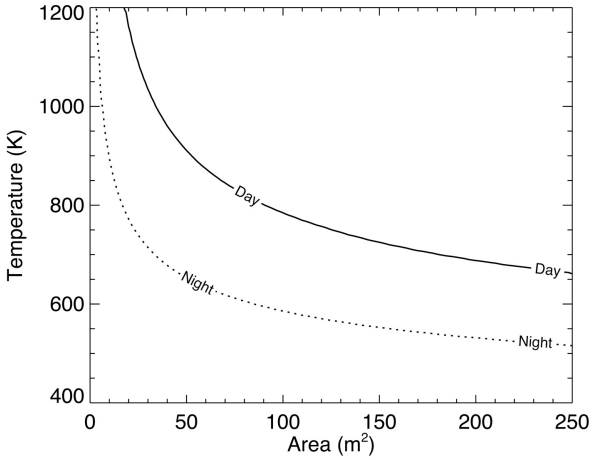

Figure 5: Theoretical 50% probability of fire detection curves derived for the VIIRS algorithm as a function of fire area and temperature using daytime and nighttime data (adapted from Schroeder *et al*. [2014]).

4.2. VALIDATION APPROACH

The validation approach adopted for the VIIRS active fire data builds on the heritage EOS/MODIS methodology, which consisted on the use of coincident reference fire data derived from higher spatial resolution sensors [Morisette *et al*., 2005; Schroeder *et al*., 2008]. However, the early afternoon orbit described by VIIRS is a major impediment limiting the use of available Landsat-class sensors (typically on ≈10am orbits) due to prohibitively large temporal separation between same-day data acquisitions [Csiszar and Schroeder, 2008]. As an alternative, reference data sets derived from airborne mapping instruments are used, complemented by field campaigns and other qualitative information originated from fire activity reports. Additionally, expert image analysts provide valuable input for the calculation of commission error rates associated with the occurrence of fire detection pixels in urban areas using available high-resolution visible imagery (e.g., Google Earth).

4.3. VALIDATION RESULTS

Data verification and validation was performed for selected sites across the globe, including dedicated field campaigns exploring small-to-medium size (<500 ha) prescribed fires (see for example: Dickinson *et al*. [2015]). Use of near-coincident airborne reference fire data shows good overall correspondence with VIIRS daytime and nighttime fire data generated for medium-to-large size wildfires as depicted in Figure 6.

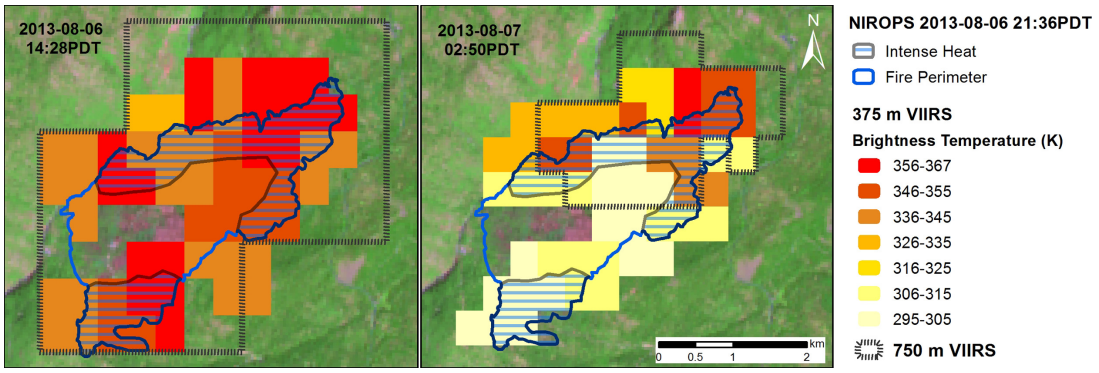

Figure 6: Airborne reference fire data (USDA/National Infrared Operations [NIROPs]) overlaid on near-coincident VIIRS daytime (left) and nighttime (right) 375 m fire detection data acquired on 06 and 07 August 2013, respectively. Outline of VIIRS 750 m baseline fire detection product is shown for reference (adapted from Schroeder *et al*. [2014]).

The occurrence of fire detection over urban areas (potential commission errors) was assessed by Schroeder *et al*. [2014] and was lower than 1.2% for nominal/high confidence pixels for all sites analyzed. Low confidence pixels responded for approximately 10% of all global fire pixels produced and showed higher occurrence of urban detections, peaking at 40% over eastern China where numerous industrial parks are found.

Comparison analyses of FRP retrievals derived using the approach above and those obtained from the VIIRS 750 m fire product (after reconciliation of the two data sets) shows good agreement (R^2=0.99) albeit with slightly (≈1%) lower values calculated for the latter. This difference is attributed to improved sampling of the background, which often results in cleaner data and higher FRP estimates. Given the spectral resolution of the M13 channel, in particular concerning the partial overlap with a CO_2 absorption band in the 4 μm region, atmospheric attenuation effects may double compared, for example, to the corresponding MODIS mid-infrared data (channels 21/22) used in the MOD14/MYD14 products (Figure 7). While this characteristic could lead to systematic underestimation of VIIRS FRP values compared to coincident MODIS data, other factors such as pixel size/geometry, data aggregation and point spread function combine to create variable effects on FRP retrievals and the resulting correlation among products (Figure 8). Detailed assessment of FRP retrievals is currently limited to field validation campaigns that are few and sparse. Data verification and validation analyses shall expand as new reference data become available.

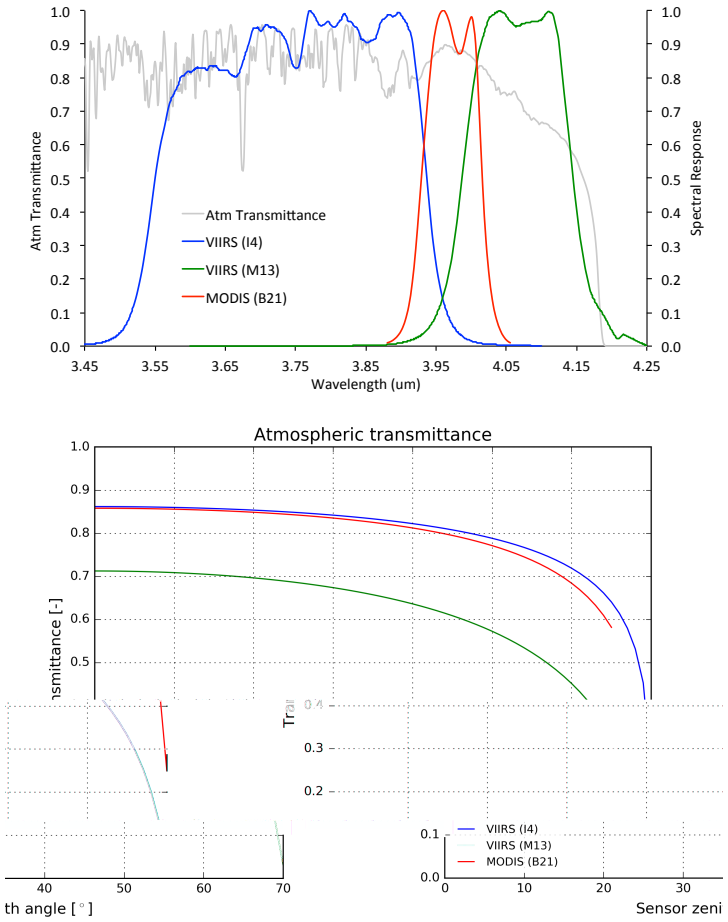

Figure 7: Spectral response functions for VIIRS I4 and M13, and MODIS B21/22 mid-infrared channels, and the corresponding atmospheric transmittance calculated using MODTRAN assuming U.S. standard atmospheric conditions (top panel). Bottom panel shows the corresponding net atmospheric transmittance as a function of the applicable VIIRS and MODIS sensor zenith angles.

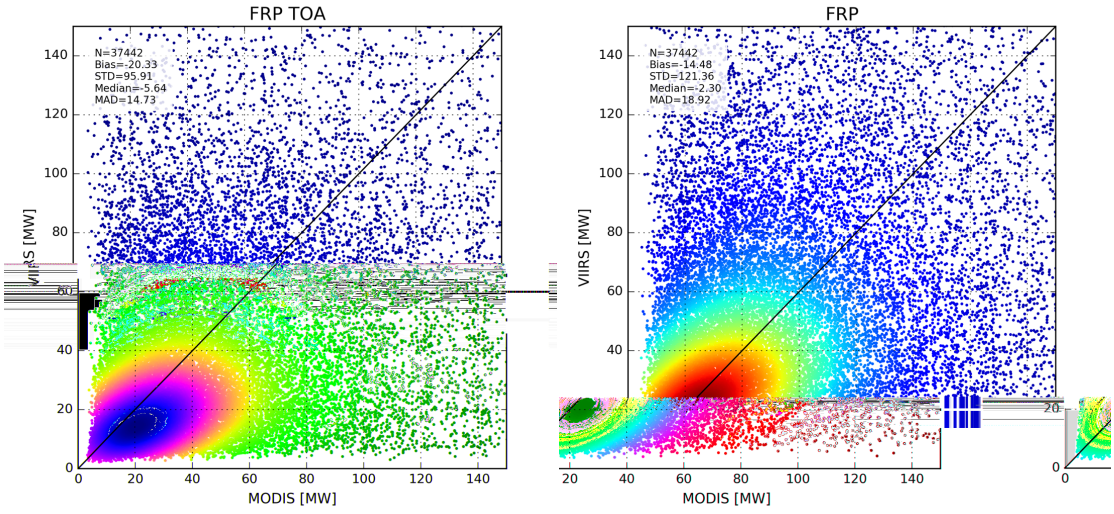

Figure 8: VIIRS M13 radiance-based FRP retrievals plotted against near-coincident Aqua/MODIS FRP (MYD14). Left panel shows top-of-atmosphere (TOA) data; right panel shows same data after atmospheric correction using MODTRAN® and MERRA 0.5º global analysis data.

5. USER GUIDANCE

VIIRS fire data users are encouraged to consult the data users guide for additional information on data accessibility and handling, and frequently asked questions.

6. ASSOCIATED PUBLICATIONS

Csiszar, I., Schroeder, W., Giglio, L., Ellicott, E., Vadrevu, K.,P., Justice, C.O., and Wind, B. (2014). Active fires from the Suomi NPP Visible Infrared Imaging Radiometer Suite: Product Status and first evaluation results. *Journal of Geophysical Research: Atmospheres*, doi: 10.1002/2013JD020453.

Giglio, L., Schroder, W., and Justice, C. (2016). The Collection 6 MODIS active fire detection algorithm and fire products. *Remote Sensing of Environment*, 178, 31-41.

Schroeder, W., Oliva, P., Giglio, L., and Csiszar, I. (2014). The new VIIRS 375 m active fire detection data product: Algorithm description and initial assessment. *Remote Sensing of Environment*, 143, 85-96.

7. REFERENCES

Csiszar, I., and Schroeder, W. (2008). Short-term observations of the temporal development of active fires from consecutive same-day ETM+ and ASTER imagery in the Amazon: Implications for active fire product validation. *IEEE Journal of Selected Topics in Applied Earth Observations and Remote Sensing*, 1(4), 248-253.

Cabrera, J., Cyamukungu, M., Stauning, P., Leonov, A., Leleux, P., Lemaire, J., *et al*. (2005). Fluxes of energetic protons and electrons measured on board the Oersted satellite. *Annales Geophysicae*, 23, 2,975-2,982.

Casadio, S., Arino, O., and Serpe, D. (2012). Gas flaring monitoring from space using ATSR instrument series. *Remote Sensing of Environment*, 116, 239-249.

Dickinson, M.B., Hudak, A.T., Zajkowski, T., Loudermilk, L.E., Schroeder W., *et al*. (2015). Measuring radiant emissions from entire prescribed fires with ground, airborne and satellite sensors – RxCADRE 2012. *International Journal of Wildland Fire*, doi: 10.1071/WF15090.

Giglio, L., Descloitres, J., Justice, C.O., and Kaufman, Y.J. (2003). An enhanced contextual fire detection algorithm for MODIS. *Remote Sensing of Environment*, 87, 273-282.

Kaufman, Y.J., Justice, C.O., Flynn, L.P., Kendall, J.D., Prins, E.M., Giglio, L., et al. (1998). Potential global fire monitoring from EOS-MODIS. *Journal of Geophysical Research*, 103 (D24), 32,215-32,238.

Lobert, J.M., and Warnatz, J. (1993). Emissions from the combustion process in vegetation. In: *Fire in the Environment: The Ecological, Atmospheric, and Climatic Importance of Vegetation Fires* (Editors: P.J. Crutzen and J.G. Goldammer), John Wiley & Sons Ltd.

Morisette, J.T., Giglio, L., Csiszar, I., and Justice, C.O. (2005). Validation of the MODIS active fire product over Southern Africa with ASTER data. *International Journal of Remote Sensing*, 26 (19), 4239-4264.

Schroeder, W., Prins, E., Giglio, L., Csiszar, I., Schmidt, C., Morisette, J.T,. and Morton, D. (2008). Validation of GOES and MODIS active fire detection products using ASTER and ETM+ data. *Remote Sensing of Environment*, 112, 2711-2726.

Wolfe, R.E., Lin, G., Nishihama, M., Tewari, K.P., Tilton, J.C., and Isaacman, A.R. (2013). Suomi NPP VIIRS prelaunch and on-orbit geometric calibration and characterization. *Journal of Geophysical Research: Atmospheres*, 118, doi:10.1002/jgrd.50873.

Wooster, M. J., Zhukov, B., and Oertel, D. (2003). Fire radiative energy for quantitative study of biomass burning: derivation from the BIRD experimental satellite and comparison to MODIS fire products. *Remote Sensing of Environment*, 86, 83–107.